Absorbing mediterranean aerosols lead to a large reduction in the solar radiation at the surface

Krzysztof M. Markowicz,[1] Piotr J. Flatau,[2,3] M. V. Ramana,[3] P. J. Crutzen,[3,4] and V. Ramanathan[3]

[1] We present direct radiometric observations of aerosol radiative forcing taken during the MINOS experiment (2001) at Finokalia Sampling Station located on North-Eastern shores of Crete, Greece. The mean value of aerosol optical thickness was 0.21 at 500 nm. Aerosols, mostly of anthropogenic origin, lead to a diurnal average reduction of 17.9 W m^{-2} in the surface solar radiation, an increase of 11.3 W m^{-2} in the atmospheric solar absorption, and an increase of 6.6 W m^{-2} in the reflected solar radiation at the top-of-the atmosphere. Thus, the present data gives observational proof for the large role of absorbing aerosols in the Mediterranean. The negative surface forcing and large positive atmospheric forcing values observed for the Mediterranean aerosols is nearly identical to the highly absorbing south Asian haze observed over the Arabian Sea.   INDEX TERMS: 0305 Atmospheric Composition and Structure: Aerosols and particles (0345, 4801); 0345 Atmospheric Composition and Structure: Pollution—urban and regional (0305); 0360 Atmospheric Composition and Structure: Transmission and scattering of radiation; 1610 Global Change: Atmosphere (0315, 0325). **Citation:** Markowicz, K. M., P. J. Flatau, M. V. Ramana, P. J. Crutzen, and V. Ramanathan, Absorbing mediterranean aerosols lead to a large reduction in the solar radiation at the surface, *Geophys. Res. Lett.*, 29(20), 1968, doi:10.1029/2002GL015767, 2002.

1. Introduction

[2] The Mediterranean Intensive Oxidant Study (MINOS) took place in 2001 on the Greek island of Crete. MINOS was a comprehensive field project to investigate anthropogenic contributions to the environment of the eastern and central Mediterranean, and provided measurements of the aerosol chemistry, microphysics, and radiation [*Lelieveld et al.*, 2002]. During the summer, the eastern part of the Mediterranean Sea is a convergent region of pollution from Central Europe, north West Africa and south Asia. The pressure distribution in July and August leads to stable northerly winds, which carry polluted air masses from Eastern and Central Europe. In the mid-troposphere, weak westerlies cause advection of air masses from the Atlantic Ocean. In addition, dust events in the Northern Africa are triggered

by synoptic disturbances in that region and are advected towards the eastern Mediterranean. In the upper troposphere air masses arrive from Atlantic Ocean or southern Asia depending on the strength of the upper level anticyclone over northern Africa.

[3] The aerosol transported from all of these sources can have a large impact on the Eastern Mediterranean Sea and lead to a change of radiative fluxes at the surface, free troposphere, and top of the atmosphere. In this study we focus on the direct aerosol forcing which is still one of the largest sources of uncertainty in climate predictions. Estimates of the radiative forcing of the Earth due to anthropogenic aerosols range from −0.4 to −2.0 W m^{-2} [*Houghton*, 2001]. Aerosols are not uniformly distributed throughout the globe, and their radiative forcing is strongly dependent on the geographical location on the Earth. For example, recent studies [*Ramanathan et al.*, 2001b] indicate that regional aerosol forcing in the Indian Ocean region are much larger and can approach −5 to −10 W m^{-2} at the top of the atmosphere and about −15 to −25 W m^{-2} at the surface. The eastern and central Mediterranean Sea in summer is under the influence of the subsiding branch of the Hadley circulation. This is responsible for the mostly clear sky conditions. Therefore, this region provides an excellent setting for studying the radiative effects of anthropogenic aerosols over the region.

[4] During MINOS we performed radiation flux measurements at the Finokalia Sampling Station (FSS) located in the north-eastern part of Crete at 35.34 N, 25.67 E about 265 m above sea level, the averaged wind speed was about 8 m/s, and grassy terrain prevented local dust mobilization [*Mihalopoulos et al.*, 1997]. Total and diffuse broadband radiative (280–2800 nm) fluxes were obtained using CM21 Kipp and Zonen pyranometers. The direct flux was measured by a CH1 Kipp and Zonen pyrheliometer mounted on a sun tracker. In order to minimize the water vapor impact on radiative forcing, we used two GUV-511 Biospherical Instruments radiometers; one of them was shadowed and another was non-shadowed. These radiometers measure visible spectrum only where water vapor absorption is very small. Together, they measure diffuse and total (sum of direct and diffuse fluxes) radiation fluxes in the visible region (400–700 nm). Aerosol optical thickness in the visible and near infrared, total columnar water vapor and ozone were obtained using the Microtops instrument [*Morys et al.*, 2001]. Using simultaneous measurements of aerosol physical (absorption and extinction) and radiative properties, we developed an aerosol model, which, in conjunction with the radiative transfer calculation successfully explains the observed solar fluxes at the surface. Also, we analyze top of the atmosphere fluxes from the Clouds and Earth

[1]Institute of Geophysics, University of Warsaw, Poland.
[2]Naval Research Laboratory, Monterey, California, USA.
[3]Center for Atmospheric Science, Scripps Institution of Oceanography, University of California, San Diego, USA.
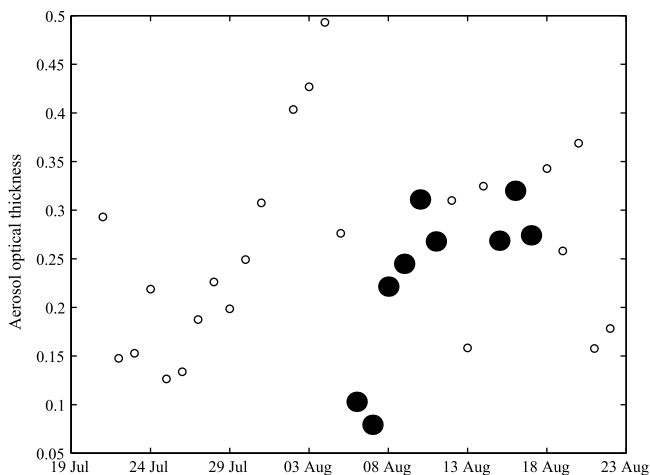[4]Max-Planck-Institute for Chemistry, Mainz, Germany.

Figure 1. Temporal variation of mean daily aerosol optical thickness at 500 nm during July and August 2001. The solid circles represent the influence of biomass burning.

Radiant Energy System (CERES) instrument onboard NASA's TERRA satellite [*Wielicki*, 1996].

2. Results

2.1. Aerosol Optical Thickness

[5] Figure 1 shows variation of the aerosol optical thickness (AOT) during July and August of 2001. AOT ranges from 0.08 to 0.5 and has significant daily and monthly variability. The average clear sky AOT values during MINOS experiment was 0.21, which is characteristic of polluted areas (e.g., the mean value for the Arabian Sea during the INDOEX experiment was about 0.25 [*Eck et al.*, 2001]). For example, the large value around August 4th is associated with increased humidity due to local orographic forcing. In general, on the basis of all the data collected, we found a large correlation between AOT and total water content ($r^2 = 0.82$), which indicates that water vapor has a strong impact on aerosol optical properties at FSS and further indicates that soluble species, such as sulfates, nitrates and oxidants organics are important components of pollution over that part of the Mediterranean Sea.

[6] Several days during our campaign (e.g. from 6 of August to 12 of August, see solid circles on Figure 1) biomass burning in Greece, Turkey and Ukraine had a strong influence on aerosol properties over Finokalia station. The absorption coefficient derived from particle soot absorption photometer during this period was about three times larger (Nikos Mihalopoulos, private communication) compared to typical values at the Finokalia station. The absorption coefficient at the Psiloritis station (1700 m above sea level) was much smaller than that at Finokalia and, therefore, we conclude, that only the boundary layer aerosol was affected by biomass burning. Psiloritis is located in central Crete, about 80 km from Finokalia.

2.2. Aerosol Forcing

[7] We basically follow the approach proposed in Satheesh and Ramanathan for obtaining forcing directly from observations [*Satheesh and Ramanathan*, 2000]. In this approach, the aerosol radiative forcing at the top-of-the atmosphere

(TOA) and at the surface are obtained from observations and the difference between the TOA and the surface forcing values define the atmospheric forcing (due to aerosol absorption of solar radiation). At the surface, the forcing is defined as the effect of aerosol on the net (down minus up) solar flux; at TOA it is the effect of aerosol on the reflected solar flux.

[8] One of the methods (not used here) to derive aerosol forcing [*Conant*, 2000] is based on empirical data only and differentiates between very clean day and polluted days (clean day is defined as without clouds and little or no pollution). The advantage is that modeling assumptions are not needed. However, during our observation period, the AOT was relatively large and large changes of water vapor were observed (between 1 and 3.5 g/cm^2) which made it difficult to find a convenient base state. Therefore, we use a hybrid technique [*Satheesh and Ramanathan*, 2000], in which the model is used to define radiative fluxes for a given tropospheric sounding under the assumption of no-clouds and no-aerosol. The surface aerosol forcing was determined for 14 clear-sky days. The radiative transfer model used in this study is Modtran version 4 [*Berk et al.*, 1998], which is based on DISORT code [*Stamnes et al.*, 1988]. The atmospheric sounding from Heraklion, Crete (00UTC) was used in the model. The vertical profiles of specific humidity was scaled by the total water vapor content from the 0.94 μm channel of Microtops. Aerosol models are defined after Optical Properties of Aerosol and Clouds (OPAC) database [*Hess et al.*, 1998]. The aerosol
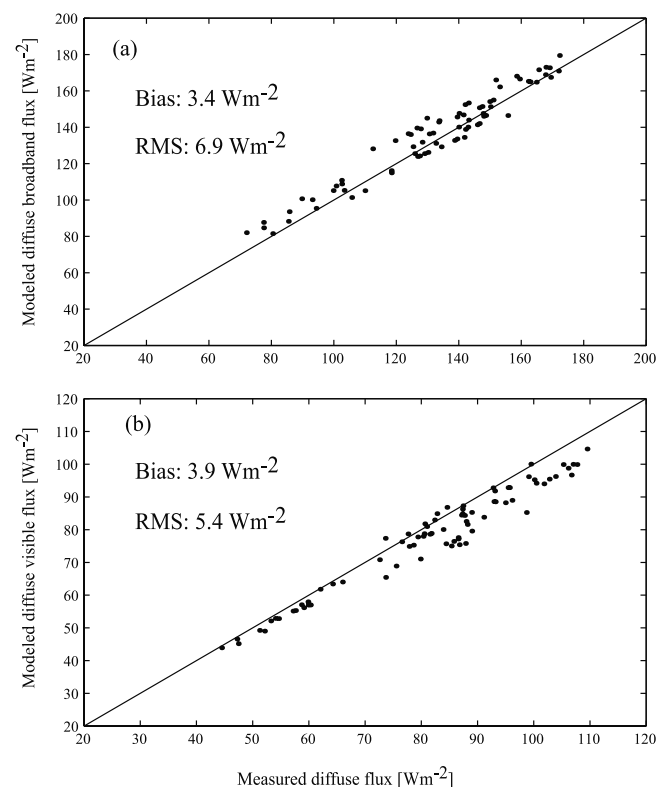

Figure 2. (a) Comparison of measured and estimated surface broadband diffuse fluxes. Solid line corresponds to perfect agreement; (b) the same as (a) but for visible (400–700 nm) range of solar spectrum.
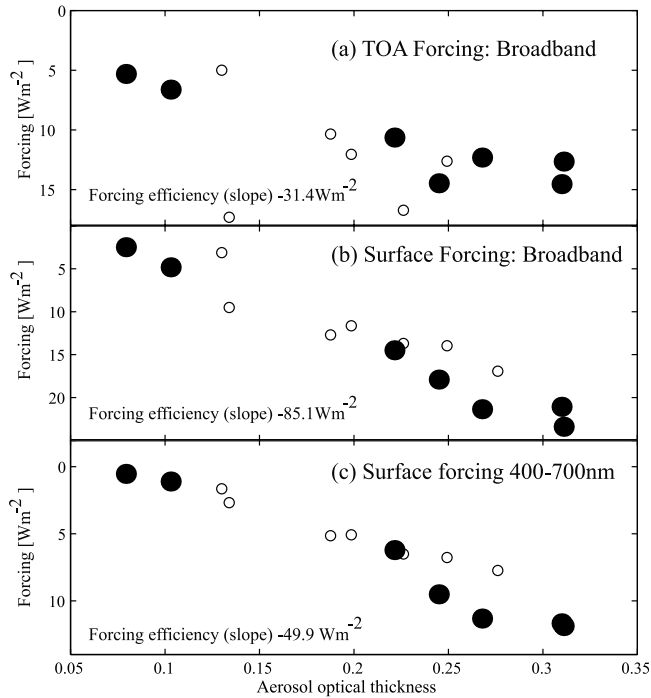
Figure 3. (a) The solar aerosol forcing at the TOA (broadband and diurnally averaged) as a function of aerosol optical depth. The solid circles represent aerosol forcing for days with fires; open circles are for days without fires. (b) The solar aerosol forcing at the Earth's surface (broadband and diurnally averaged); (c) The same as (b) but for visible (400–700 nm) range of solar spectrum.

model was constrained by AOT in 4 channels and Ångstrom exponent. To calculate the incoming fluxes we assumed that the island broadband albedo was 0.15.

[9] Figure 2a shows comparison of broadband diffuse fluxes between model and observations. The model results overestimate measured fluxes by 3.4 W m^{-2}. The root mean square (rms) error is 6.7 W m^{-2} but this difference is within instrumental uncertainty. The comparison of the visible range solar radiation is shown on Figure 2b. In this case the model results underestimates observation by 3.9 W m^{-2} (rms 5.4 W m^{-2}). Similar differences [*Conant*, 2000; *Satheesh et al.*, 1999] were documented previously.

[10] The top of the atmosphere (TOA) forcing was obtained from CERES (the resolution of CERES is 20 km at nadir) on board of the TERRA satellite. CERES measures radiances, which are converted to fluxes using ERBE-like angular distribution models [*Loeb et al.*, 2000]. In this study we use Edition 1 ES-8 of CERES data [*Wielicki*, 1996]. Our interest in this study is the Mediterranean Sea and, hence, we adopt fluxes over the sea, about 30–50 km from

Finokalia. The view angle was limited to less then 60 degrees (to avoid very large viewing angles). The instantaneous fluxes were converted to diurnal mean values using the Modtran radiative transfer model. The conversion factor varied from 1.7 to 1.8. The TOA forcing as a function of mean diurnal optical depth at 500 nm is shown in Figure 3a. The flux does not asymptote to zero for zero optical depth due to offset errors in observations and also due to model errors. However, the slope obtained from the linear fit to the forcing is independent of this bias. The slope, which is the aerosol forcing efficiency, is −31.4 W m^{-2} with an error of about 10.1 W m^{-2}. Without the two outlier points (the open dots with a forcing of −17 W m^{-2}) the efficiency is −39.4 ± 12.8 W m^{-2}. The forcing efficiency (all days) multiplied by averaged clear-sky AOT (0.21) is −6.6 ± 2.1 W m^{-2} (see Table 1) but without the two outlier points it is −8.3 ± 2.7 W m^{-2} (this value has * in front in Table 1). We do not have a good explanation for the discrepancy, but a possible source of error is improper classification of clear sky conditions (cloud contamination) and the state of the sea including white caps contribution.

[11] The surface aerosol forcing is shown in Figure 3b for broadband flux and in Figure 3c for the visible solar flux (400 to 700 nm). To estimate the total flux we used the sum of the direct and the diffuse components. Figure 3b shows the daily average aerosol forcing as a function of aerosol optical depth. Using the same "slope" method we derive the mean aerosol forcing for clear sky to be −17.9 ± 2.1 W m^{-2}. The mean aerosol surface forcing efficiency during MINOS is −85.1 W m^{-2} (see Table 1) with 10 W m^{-2} uncertainty. This forcing is only about 15% larger of that reported previously [*Satheesh and Ramanathan*, 2000] for polluted region of northern Indian Ocean (−75 W m^{-2}). Figure 3c shows aerosol forcing in the visible range of solar spectrum. The mean aerosol forcing efficiency is −49.9 W m^{-2} and the diurnal reduction of solar radiation is 10.5 W m^{-2}. An important parameter regulating the aerosol forcing is the vertical distribution of the single scattering albedo (SSA), which was not continuously measured during MINOS. The best agreement with the observed forcing and with observed diffuse fluxes at the surface were obtained, when we assumed a column averaged SSA of 0.87. However we emphasize that the main thrust of this paper is on the observed forcing and the model results are only an ancillary point of this paper.

[12] The difference between the cases with and without fires on aerosol forcing is clearly shown in Figures 3b and 3c. Solid circles correspond to days with fires and open circles correspond to days without fires; aerosol efficiency is −87.9 W m^{-2} (fires) and −70.7 W m^{-2} for solar and −51.8 W m^{-2} (fires) and −39.4 W m^{-2} for visible (see Table 2). For days without fires aerosol forcing efficiency is in good agreement with the INDOEX values [*Conant*, 2000; *Satheesh and Ramanathan*, 2000]. Scaling the visible

Table 1. Comparison of Mean Aerosol Direct Radiative Forcing (W m^{-2}) Between Observations and Model Results

Method	TOA	Surface Broadband	Surface Visible
Observation	−6.6 ± 2.1*−8.3 ± 2.7	−17.9 ± 2.7	−10.5 ± 1.7
Model, SSA = 0.87	−5.9	−18.3	−10.5

[a] The value indicated by * is without the two outlier points (see text).

Table 2. Comparison of the Mean Surface Aerosol Forcing Efficiency (W m^{-2}) During Days With and Without Fires

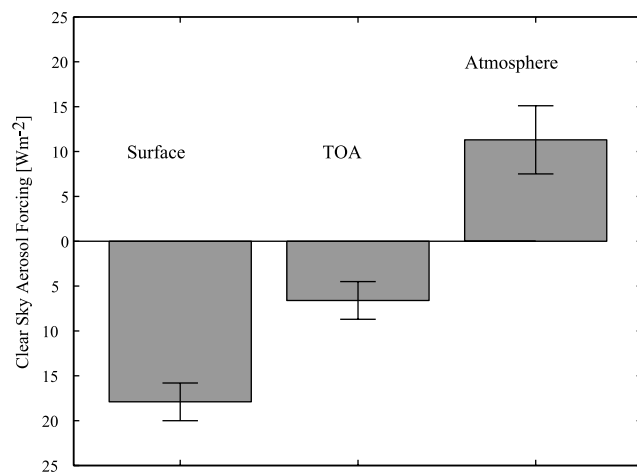| Period	Broadband	Visible	Broadband calculated from visible spectrum
Fires	−87.9	−51.8	−90.1
No-Fires	−70.7	−39.4	−68.6

Figure 4. The surface, TOA, and atmospheric aerosol forcing.

forcing in Figure 3c to broadband forcing (using the radiative transfer code) one obtains the broadband forcing efficiency -90.1 W m^{-2} (fires) and -68.6 W m^{-2} (no fires), which indicates excellent consistency between the broadband and the visible measurements.

[13] An important finding (see Table 2) is that during episodes of biomass burning (solid circles on Figures 3b and 3c) the forcing efficiency is much larger. The difference between the forcing efficiency at the surface for absorbing and less-absorbing aerosols is about -21 W m^{-2} for broadband and -12 W m^{-2} for visible solar spectrum range.

[14] On the basis of our analyses we can derive the ratio of the surface to the TOA aerosol forcing, which is an index for the aerosol absorbing efficiency. For MINOS this ratio is 2.7. For comparison, a model with sulfate or sea salt only produces 1.5, when soot is added to the aerosol model the ratio increases to 3.7 for SSA 0.87, thus we conclude that other component, possibly dust, contributes to absorption. Also, the mean atmospheric absorption during MINOS (TOA forcing minus surface forcing) is 11.3 ± 3.8 W m^{-2} (Figure 4).

[15] The large negative surface aerosol forcing and the associated tropospheric heating may have several important feedbacks. A large reduction of solar radiation absorbed at the surface (diurnal average reduction up to 18 W m^{-2} and about 65 W m^{-2} during local noon) may have an impact on the surface evaporation [*Ramanathan et al.*, 2001a], static stability of lower troposphere pod [*Podgorny et al.*, 2000; *Vogelmann et al.*, 2001]; suppression of convection by soot heating. It might also lead to a decrease of cloud cover and precipitation which was observed during the last decade [*Long et al.*, 2000].

References

Berk, A., L. S. Bernstein, G. P. Anderson, P. K. Acharya, D. C. Robertson, J. H. Chetwynd, and S. M. Adler-Golden, MODTRAN cloud and multi-

ple scattering upgrades with application to AVIRIS, *Remote. Sens. Environ.*, *65*, 367–375, 1998.

Conant, W. C., An observational approach for determining aerosol surface radiative forcing: Results from the first field phase of INDOEX, *J. Geophys. Res.*, *105*, 15,347–15,360, 2000.

Eck, T. F., B. N. Holben, O. Dubovik, A. Smirnov, I. Slutsker, J. M. Lobert, and V. Ramanathan, Column-integrated aerosol optical properties over the Maldives during the northeast monsoon for 1998–2000, *J. Geophys. Res.*, *106*, 28,555–28,566, 2001.

Hess, M., P. Koepke, and I. Schult, Optical properties of aerosols and clouds: The software package OPAC, *Bull. Amer. Meteorol. Soc.*, *79*, 831–844, 1998.

Houghton, J. T., *Climate change 2001: The scientific basis: Contribution of Working Group I to the third assessment report of the Intergovernmental Panel on Climate Change*, 881 pp., Cambridge University Press, Cambridge, U.K., New York, 2001.

Lelieveld, J., H. Berresheim, S. Borrmann, P. J. Crutzen, F. J. Dentener, H. Fischer, J. de Gouw, J. Feichter, P. J. Flatau, J. Heland, R. Holzinger, R. Korrmann, M. Lawrence, Z. Levin, K. Markowicz, N. Mihalopoulos, A. Minikin, V. Ramanathan, M. de Reus, G. J. Roelofs, H. A. Scheeren, J. Sciare, H. Schlager, M. Schultz, P. Siegmund, B. Steil, P. Stier, M. Traub, J. Williams, and H. Ziereis, Global air pollution crossroads over the Mediterranean, In press, *Science,* 2002.

Loeb, N. G., F. Parol, J. C. Buriez, and C. Vanbauce, Top-of-atmosphere albedo estimation from angular distribution models using scene identification from satellite cloud property retrievals, *J. Climate*, *13*, 1269–1285, 2000.

Long, M., D. Entekhabi, and S. E. Nicholson, Interannual variability in rainfall, water vapor flux, and vertical motion over West Africa, *J. Climate*, *13*, 3827–3841, 2000.

Mihalopoulos, N., E. Stephanou, M. Kanakidou, S. Pilitsidis, and P. Bousquet, Tropospheric aerosol ionic composition in the Eastern Mediterranean region, *Tellus B*, *49*, 314–326, 1997.

Morys, M., F. M. Mims, S. Hagerup, S. E. Anderson, A. Baker, J. Kia, and T. Walkup, Design, calibration, and performance of MICROTOPS II handheld ozone monitor and Sun photometer, *J. Geophys. Res.*, *106*, 14,573–14,582, 2001.

Podgorny, I. A., W. Conant, V. Ramanathan, and S. K. Satheesh, Aerosol modulation of atmospheric and surface solar heating over the tropical Indian Ocean, *Tellus B*, *52*, 947–958, 2000.

Ramanathan, V., P. J. Crutzen, J. T. Kiehl, and D. Rosenfeld, Atmosphere-Aerosols, climate, and the hydrological cycle, *Science*, *294*, 2119–2124, 2001a.

Ramanathan, V., P. J. Crutzen, J. Lelieveld, A. P. Mitra, D. Althausen, J. Anderson, M. O. Andreae, W. Cantrell, G. R. Cass, C. E. Chung, A. D. Clarke, J. A. Coakley, W. D. Collins, W. C. Conant, F. Dulac, J. Heintzenberg, A. J. Heymsfield, B. Holben, S. Howell, J. Hudson, A. Jayaraman, J. T. Kiehl, T. N. Krishnamurti, D. Lubin, G. McFarquhar, T. Novakov, J. A. Ogren, I. A. Podgorny, K. Prather, K. Priestley, J. M. Prospero, P. K. Quinn, K. Rajeev, P. Rasch, S. Rupert, R. Sadourny, S. K. Satheesh, G. E. Shaw, P. Sheridan, and F. P. J. Valero, Indian Ocean Experiment: An integrated analysis of the climate forcing and effects of the great Indo-Asian haze, *J. Geophys. Res.*, *106*, 28,371–28,398, 2001b.

Satheesh, S. K., and V. Ramanathan, Large differences in tropical aerosol forcing at the top of the atmosphere and Earth's surface, *Nature*, *405*, 60–63, 2000.

Satheesh, S. K., V. Ramanathan, L. J. Xu, J. M. Lobert, I. A. Podgorny, J. M. Prospero, B. N. Holben, and N. G. Loeb, A model for the natural and anthropogenic aerosols over the tropical Indian Ocean derived from Indian Ocean Experiment data, *J. Geophys. Res.*, *104*, 27,421–27,440, 1999.

Stamnes, K., S. C. Tsay, W. Wiscombe, and K. Jayaweera, Numerically stable algorithm for discrete-ordinate-method radiative transfer in multiple scattering and emitting layered media, *Appl. Opt.*, *27*, 2502–2509, 1988.

Vogelmann, A. M., V. Ramanathan, and I. A. Podgorny, Scale dependence of solar heating rates in convective cloud systems with implications to general circulation models, *J. Climate*, *14*, 1738–1752, 2001.

Wielicki, B. A., Clouds and the Earths Radiant Energy System (CERES) - an Earth Observing System Experiment, *Bull. Amer. Meteorol. Soc.*, *77*, 1590, 1996.

—————————————

K. M. Markowicz, Institute of Geophysics, University of Warsaw, Poland. (kmark@igf.fuw.edu.pl)

P. J. Flatau, UCAR visiting scientist, Naval Research Laboratory, Monterey, California, USA.

M. V. Ramana and V. Ramanathan, Center for Atmospheric Science, Scripps Institution of Oceanography, University of California, San Diego, USA.

P. J. Crutzen, Max-Planck-Institute for Chemistry, Mainz, Germany.